

#### **PAPER**

# 4D *in vivo* dosimetry for a FLASH electron beam using radiation-induced acoustic imaging

To cite this article: Kristina Bjegovic et al 2024 Phys. Med. Biol. 69 115053

View the article online for updates and enhancements.

#### You may also like

- FLASH radiotherapy: technical advances, evidence of the FLASH effect and mechanistic insights
   Mustapha Chaoui, Othmane Bouhali and Yahya Tayalati
- Mathematical analysis of FLASH effect models based on theoretical hypotheses
   Ankang Hu, Wanyi Zhou, Rui Qiu et al.
- Physics and biology of ultrahigh dose-rate (FLASH) radiotherapy: a topical review Nolan Esplen, Marc S Mendonca and Magdalena Bazalova-Carter





Increase your workflow efficiency without sacrificing quality.



Maximize your measurement accuracy and precision.



Have confidence in the QA software trusted among top treatment facilities.

CLICK TO LEARN MORE

For over 32 years, RIT has provided medical physicists with an impressive range of convenient QA software packages to fit both your needs and budget. The RIT Family of Products software provides patient, machine, and imaging QA for TG-142, TG-148, TG-135, as well as automated phantom analysis for diagnostic imaging. RIT software utilizes a combination of powerful, robust routines in a user-friendly interface to maximize the efficiency and precision of your measurements. Easily export your analysis data as customizable reports or to the RIT*trend*<sup>TM</sup> statistical database for large-scale tracking and trending over time.

Visit radimage.com to find your perfect QA software solution today.

Email: sales@radimage.com

Call: 1(719) 590 - 1077, Opt. 4

©2025, Radiological Imaging Technology, Inc.

## Physics in Medicine & Biology





22 February 2024

REVISED 23 April 2024

ACCEPTED FOR PUBLICATION 9 May 2024

PUBLISHED

31 May 2024

## **PAPER**

## 4D in vivo dosimetry for a FLASH electron beam using radiation-induced acoustic imaging

Kristina Bjegovic¹ أو, Leshan Sun¹, Prabodh Pandey² أو, Veljko Grilj⁵, Paola Ballesteros-Zebadua⁵،6, Ryan Paisley<sup>5</sup>, Gilberto Gonzalez<sup>7</sup>, Siqi Wang<sup>1</sup>, Marie Catherine Vozenin<sup>5,8</sup>, Charles L Limoli<sup>4</sup> and Shawn (Liangzhong) Xiang<sup>1,2,3,</sup>

- The Department of Biomedical Engineering, University of California, Irvine, CA 92617, United States of America
- Department of Radiological Sciences, University of California, Irvine, Irvine, CA 92697, United States of Americaica
- Beckman Laser Institute & Medical Clinic, University of California, Irvine, Irvine, CA 92612, United States of America
- Department of Radiation Oncology, University of California, Irvine, Irvine, CA 92697-2695, United States of America
- Laboratory of Radiation Oncology, Radiation Oncology Service and Oncology Department, Lausanne University Hospital and University of Lausanne, Lausanne, Switzerland
- Laboratory of Medical Physics, National Institute of Neurology and Neurosurgery, Mexico City, Mexico
- Department of Radiation Oncology, University of Oklahoma Health Sciences Center, Oklahoma City, OK 73104, United States of
- 8 Sector of Radiobiology applied to Radiation Oncology, Radiation Oncology Service, Geneva University Hospital and University of Geneva, Geneva, Switzerland
- Author to whom any correspondence should be addressed.

E-mail: liangzhx@hs.uci.edu

Keywords: radiation therapy, FLASH therapy, in vivo dosimetry, radiation-induced acoustic imaging (RAI) Supplementary material for this article is available online

Objective. The primary goal of this research is to demonstrate the feasibility of radiation-induced acoustic imaging (RAI) as a volumetric dosimetry tool for ultra-high dose rate FLASH electron radiotherapy (FLASH-RT) in real time. This technology aims to improve patient outcomes by accurate measurements of in vivo dose delivery to target tumor volumes. Approach. The study utilized the FLASH-capable eRT6 LINAC to deliver electron beams under various doses  $(1.2 \text{ Gy pulse}^{-1} \text{ to } 4.95 \text{ Gy pulse}^{-1})$  and instantaneous dose rates  $(1.55 \times 10^5 \text{ Gy s}^{-1} \text{ to})$  $2.75 \times 10^6$  Gy s<sup>-1</sup>), for imaging the beam in water and in a rabbit cadaver with RAI. A custom 256-element matrix ultrasound array was employed for real-time, volumetric (4D) imaging of individual pulses. This allowed for the exploration of dose linearity by varying the dose per pulse and analyzing the results through signal processing and image reconstruction in RAI. Main Results. By varying the dose per pulse through changes in source-to-surface distance, a direct correlation was established between the peak-to-peak amplitudes of pressure waves captured by the RAI system and the radiochromic film dose measurements. This correlation demonstrated dose rate linearity, including in the FLASH regime, without any saturation even at an instantaneous dose rate up to  $2.75 \times 10^6$  Gy s<sup>-1</sup>. Further, the use of the 2D matrix array enabled 4D tracking of FLASH electron beam dose distributions on animal tissue for the first time. Significance. This research successfully shows that 4D in vivo dosimetry is feasible during FLASH-RT using a RAI system. It allows for precise spatial ( $\sim$ mm) and temporal (25 frames s<sup>-1</sup>) monitoring of individual FLASH beamlets during delivery. This advancement is crucial for the clinical translation of FLASH-RT as enhancing the accuracy of dose delivery to the target volume the safety and efficacy of radiotherapeutic procedures will be improved.

#### 1. Introduction

In vivo dosimetry is crucial in radiotherapy to ensure accurate dose delivery and minimize risks to patients, yet it remains largely unavailable in clinical practice (Mijnheer et al 2013, Olaciregui-Ruiz et al 2020). While Cerenkov radiation provides a viable option for surface *in vivo* dosimetry (Glaser *et al* 2013, 2014, Jarvis *et al* 2014), it falls short in monitoring deep-seated tumors. Recent advancements in radiation-induced acoustic imaging (RAI) have shown promise for *in vivo* dosimetry in treating tumors deep inside the patient (Ahmad *et al* 2015, Patch *et al* 2016, Kim *et al* 2017, Lei *et al* 2018, Hickling *et al* 2018b, Samant *et al* 2020, Zheng *et al* 2020, Gonzalez *et al* 2023, Caron *et al* 2023, Sun *et al* 2023, Zhang *et al* 2023).

RAI began its journey with the use of a single transducer in proof-of-concept experiments, laying the foundation for this innovative technology (Xiang et al 2012). This initial phase involved using a commercial ultrasound transducer, immersed in water and rotated around the beam, to facilitate a basic 2D reconstruction of the beam shape (Hickling et al 2018a). It established the crucial relationship between acoustic wave amplitude and radiation dose, marking a significant step forward in real-time, in vivo dosimetry (Lei et al 2018, Wang et al 2020, Jiang et al 2022, Sun et al 2023). As the technology evolved, the use of linear arrays was introduced, enabling 2D imaging capabilities without the need for mechanical scanning (Oraiqat et al 2020, Zhang et al 2020). This advancement streamlined the process, allowing for more efficient and accurate tracking of radiation beams in two dimensions. Recent studies have further advanced RAI by employing matrix arrays, which have opened the door to 3D imaging (Wang et al 2020, Jiang et al 2022, Zhang et al 2023). However, the majority of these advancements have been focused on conventional radiotherapy, where the technology has been applied to track and monitor radiation in more traditional treatment settings.

FLASH radiotherapy (FLASH-RT), involves the use of ultra-high dose rates ( $\geqslant$ 100 Gy s<sup>-1</sup> mean dose rates) and has been shown to minimize toxicity to the surrounding healthy tissues without compromising tumor control (Soto *et al* 2020, Montay-Gruel *et al* 2021). Despite promising preclinical results across various tumor types and the potential to enhance patient quality of life (Bourhis *et al* 2019, Simmons *et al* 2019, Vozenin *et al* 2019, Levy *et al* 2020), the translation of FLASH-RT into clinical practice is hindered by the lack of real-time, *in vivo* dosimetry (Ashraf *et al* 2020, El Naqa *et al* 2022). This gap is particularly critical given current trends toward hypofractionation, and the fact that FLASH may soon be used to deliver fewer and higher doses/fraction safely compared to conventional radiotherapy. Despite these potential benefits, rapid dose delivery incurs a heightened risk of inaccurate dose delivery and/or beam mispositioning.

Based on the foregoing, simulation studies have already indicated the potential of RAI in capturing images of FLASH beams, applicable to both protons (Kim *et al* 2023) and electrons (Ba Sunbul *et al* 2021). Notably, recent experimental research has showcased the use of RAI with two linear arrays in an orthogonal setup for detecting the edges of FLASH electron beams up to 25 cGy, proving its feasibility (Oraiqat *et al* 2020). Despite RAI's demonstrated success in standard radiotherapy contexts, its application to the dynamic and intricate demands of FLASH-RT, particularly for achieving real-time, volumetric (4D) imaging, is still an emerging field awaiting further exploration.

Our research pushes the boundaries of RAI in FLASH-RT by employing a  $16 \times 16$  element 2D matrix array for the first time, achieving real-time 3D imaging for a single electron pulses. This study successfully demonstrated dose rate linearity without saturation at dose rates up to  $2.75 \times 10^6$  Gy s<sup>-1</sup>. This breakthrough in 4D tracking of FLASH electron beam dose distributions in animal models heralds a new era in radiotherapy dosimetry, promising significant improvements in treatment precision and safety.

#### 2. Materials and methods

#### 2.1. Radiation induced acoustic signal generation

The creation of an acoustic signal begins when radiation dose is absorbed by tissue, leading to a localized increase in temperature (Xiang *et al* 2012). This rise in temperature causes the tissue to expand. Subsequently, when the beam pulse ceases and no additional energy is deposited, the temperature falls, resulting in tissue contraction (Zeng *et al* 2007, Yang *et al* 2007a, 2007b, Lao *et al* 2008, Xiang *et al* 2009, 2013, Wang and Hu 2012, Wang *et al* 2012, Hu *et al* 2019, Samant *et al* 2020). This process of thermoelastic expansion and contraction produces 3D acoustic waves (Hickling *et al* 2018b, Samant *et al* 2020, Yan and Xiang 2024). These waves adhere to the wave equation, particularly under conditions of thermal confinement (Wang and Hu 2012):

$$\left(\nabla^2 - \frac{1}{v_s^2} \frac{\partial^2}{\partial t^2}\right) p\left(\vec{r}, t\right) = -\frac{\beta}{C_p} \frac{\partial H\left(\vec{r}, t\right)}{\partial t}$$
 (1)

where  $v_s$  is the speed of sound in the target medium,  $p(\vec{r}, t)$  is the acoustic pressure rise at time t and location  $\vec{r}$ ,  $\beta$  is the target volume thermal coefficient,  $C_p$  is the specific heat capacity of the target medium at a

constant pressure, and  $H(\vec{r},t)$  is the heating function (Samant *et al* 2020). The heating function  $H(\vec{r},t)$  can be written as:

$$H(\vec{r},t) = \eta_{th} D(\vec{r},t) \rho \tag{2}$$

as a function of D, the deposited dose per unit time, where  $\eta_{th}$  is the percentage of the absorbed energy or dose that converts into heat, and  $\rho$  is the density of the target tissue (Wang *et al* 2020). Thus, equation (1) can be rewritten, describing the generated pressure waves as a function of the dose deposited into the tissue:

$$\left(\nabla^2 - \frac{1}{\mathbf{v}_s^2} \frac{\partial^2}{\partial t^2}\right) p\left(\vec{r}, t\right) = -\frac{\beta \eta_{\text{th}} \rho}{C_p} \frac{\partial D\left(\vec{r}, t\right)}{\partial t}.$$
 (3)

The acoustic pressure p(r,t) detected at the transducer position r and time t can be expressed by Hickling  $et\ al\ (2018b)$ :

$$\mathbf{p}(\mathbf{r},t) = \frac{1}{4\pi v_{s}^{2}} \int d\mathbf{r}' \frac{1}{|\mathbf{r} - \mathbf{r}'|} \Gamma \eta_{th} \rho \frac{\partial D_{\mathbf{r}}(\mathbf{r}',t')}{\partial t'} \bigg|_{t'=t-\frac{|\mathbf{r} - \mathbf{r}'|}{r}}$$
(4)

where  $\Gamma$  is the Grüneisen parameter defined as:  $\Gamma = \frac{\beta K_T}{C_v \rho}$ . where  $\beta$  is the volumetric thermal expansion coefficient, and  $K_T$  is the isothermal bulk modulus. Meanwhile, the initial acoustic pressure  $p_0(r)$  induced by radiation can be obtained by Zhang *et al* (2020):

$$\mathbf{p}_{0}(\mathbf{r}) = \Gamma \eta_{\text{th}} \rho D_{\mathbf{p}}(\mathbf{r}) \tag{5}$$

where  $D_p(r) = D_r(r,t) \tau_p$  is the local energy deposition due to a single electron pulse with a pulse duration of  $\tau_p$ . The pixel intensity within the RAI image, reconstructed from captured radiation-induced acoustic signals, reflects the initial acoustic pressure. Consequently, the relative intensity image, provides crucial insights into (1) the location of the electron beam and (2) the quantity of dose delivered to the target.

#### 2.2. Experimental setup

In our study, we employed a prototype electron beam linear accelerator (LINAC, the Oriatron eRT6 from PMB-Alcen, France) at Lausanne University Hospital (Jaccard et al 2018). This LINAC is equipped for both conventional RT and FLASH RT, featuring adjustable settings including dose per pulse (ranging from less than 15 cGy to 20 Gy), pulse width (500 ns to 4 µs), repetition frequency (5–250 Hz), and electron gun voltage (0–300 V). For monitoring beam output during treatments, we attached a beam current transformer (BCT, Bergoz Instrumentation, France). The BCT's output was divided into two: one for the beam monitoring system used in FLASH-RT experiments for beam counting, and another for triggering synchronized radiation-induced acoustic (RA) signal acquisition. This setup enabled the capture of RA signals from individual irradiation pulses. Graphite collimators were used to focus the beam before it reached the acquisition zone, with a rectangular collimator employed for gathering linearity data. We utilized two different types of transducers for RA signal acquisition in our experiments: a single-element ultrasound transducer (A389S-SU, Olympus INS, Japan) and a custom 256-element matrix array (Photosound Inc, USA). The point transducer, with a 500 kHz center frequency and 60% bandwidth, was submerged in a water tank for linearity studies, as depicted in figure 2. Signals from individual pulses were amplified using a 40 dB preamplifier (5660B Ultrasonic Preamplifier Panametrics-NDT, Olympus, Japan) and recorded with an oscilloscope (DSOX2024A, Keysight Technologies, USA). Conversely, the 256-element matrix array, with a 1 MHz center frequency and 60% bandwidth, facilitated real-time 3D imaging and enabled volumetric reconstructions of single pulse dose depositions in both a water tank and rabbit tissue (figures 3–6). Raw RA signals from each array element were simultaneously amplified and captured using a custom 256-channel data acquisition system (Legion ADC, Photosound, USA), as illustrated in figure 1. This approach allowed for immediate 3D reconstructions from individual pulses without mechanical scanning. All data processing and reconstruction were performed in MATLAB (R2021b, MathWorks Inc, USA), using a universal back-projection (UBP) method (Xu and Wang 2005).

#### 2.3. Comparison between RA measurement and film dosimetry

To establish a gold standard for comparison, we used radiochromic film (Gafchromic EBT3 film, Ashland Advanced Materials, USA) to validate our radiation-induced acoustic measurements. In the FLASH-RT experiments, we adjusted the source-to-surface distance (SSD) to administer different doses, a technique also commonly used in clinical settings. For each SSD setting, a single pulse of the electron beam irradiated the

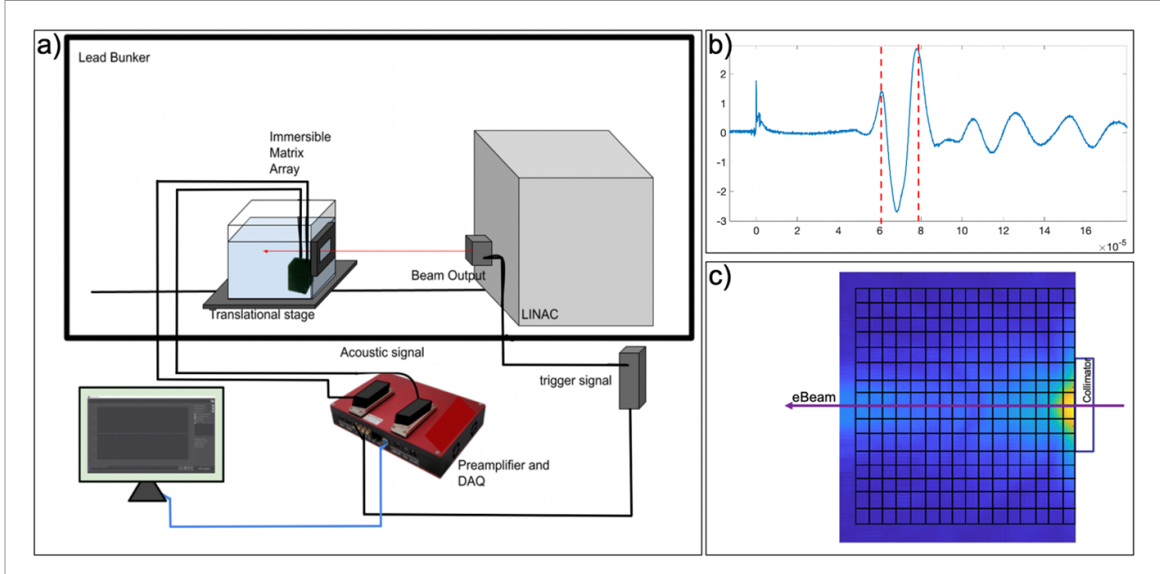


**Figure 1.** Representative RAI system and RA signals. (a) displays the RAI system setup for 256 multi-channel acquisitions with 256 element matrix arrays (c) used for studies in water and *in vivo*. (b) shows a typical RA signal, with dotted lines indicating signal time of flight estimations. (c) illustrates a maximum intensity projection of dose deposition in water in the *XY* plane, indicating the 256-element matrix array's orientation for 3D imaging.

film, with the process repeated on fresh film for both averaging and individual dose per pulse assessments. These film measurements were then compared to the radiation-induced acoustic data obtained under identical beam collimation and power, and at the same depth in the water tank.

#### 2.4. Signal processing and 3D image reconstruction

In our study, we employed the UBP algorithm by using the following equation (Xu and Wang 2005):

$$p_{0}\left(\vec{r}\right) = \int_{c} \left[ 2p\left(\vec{r}_{d}, t\right) - 2t \frac{\partial p\left(\vec{r}_{d}, t\right)}{\partial t} \right] \frac{d\Omega}{\Omega_{0}} \bigg|_{t = |\vec{r}_{d} - \vec{r}|_{V_{s}}}$$
(6)

where  $p_0(\vec{r})$  is the reconstructed initial pressure at position  $\vec{r}$ ,  $p(\vec{r}_d, t)$  is the measured radiation induced acoustic pressure at detector position  $r_d$  and time  $t = |\vec{r}_d - \vec{r}| v_s$ , and  $\Omega_0$  is the solid angle that the transducer surface S covers.

The radiation-induced acoustic signals were processed using a bandpass filter aligned with the bandwidth of the ultrasound transducer. Additionally, to enhance the signal-to-noise ratio (SNR), the signals were averaged. Although single pulse reconstructions were also performed, 25 frames were specifically utilized for this averaging process which leading to higher SNR. The size of the 256-element matrix array was  $4.8~\mathrm{cm} \times 4.8~\mathrm{cm}$  and a reconstruction grid of  $4.8~\mathrm{cm} \times 4.8~\mathrm{cm} \times 6~\mathrm{cm}$  above the transducer was created with a voxel resolution of  $400~\mu\mathrm{m}$ . All reconstruction was run in MATLAB.

#### 2.5. TOPAS simulation

To accurately model the electron dose deposition, we employed TOPAS, a Monte Carlo tool widely used in radiation therapy research. A custom code was tailored to replicate the beam energy spectrum and percent depth-dose characteristics of the eRT6 prototype LINAC, based on the reference dose profiles established in a comprehensive commissioning study conducted by Jaccard *et al* (2018). A brass collimator was integrated into the simulation setup to emulate the field geometry, maintaining similar SSD and aperture size. The simulation conducted 1000 000 electron histories to enhance statistical reliability. The deposited dose distribution was collected using a water-material binning component, employing a voxel resolution of 0.5 mm to capture fine-scale variations. Subsequently, the dose information was exported to MATLAB in CSV format.

#### 3. Results

#### 3.1. Dose linearity study in FLASH regime

To fully harness the potential of FLASH-RT, it is essential to monitor individual pulses accurately, as variations in these pulses can significantly affect treatment outcomes (El Naqa *et al* 2022). We investigated

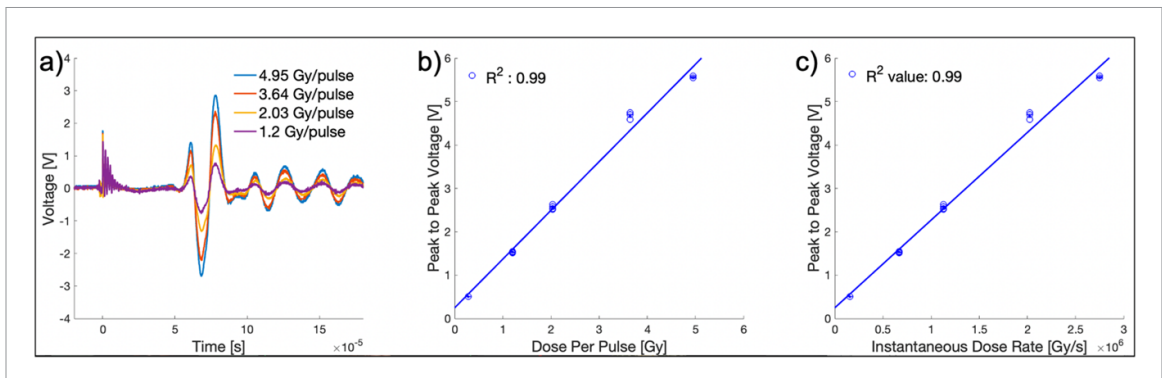


**Figure 2.** Linearity evaluation of radiation-induced acoustic measurements in the FLASH regime. (a) Demonstrates typical RA signals obtained by varying the radiation dose from 1.2 Gy pulse $^{-1}$  to 4.94 Gy pulse $^{-1}$ . (b) Illustrates the relationship between the peak-to-peak amplitude of the RA signal and the dose per pulse, revealing excellent linearity within the FLASH regime. (c) Shows the correlation between the peak-to-peak amplitude of the RA signal and the instantaneous dose rate, reaching up to  $3*10^6$  Gy s $^{-1}$ . Linear fits for both datasets exhibit  $R^2$  values exceeding 0.99, indicating high linearity.

the linearity between Radiation-Induced Acoustic (RA) signals and radiation dosimetry within the FLASH regime. Using a point transducer system, we varied the dose in experiments by changing the SSD, a method akin to clinical practices. The experiment involved moving the translational stage, which held the water tank and submerged transducer, to different SSDs, thus varying the dose per pulse. At each SSD, the FLASH electron beam, with a pulse width of 1.8  $\mu$ s, was fired five times. We conducted parallel radiochromic film irradiation at each distance to compare with the RA signal amplitude, establishing a gold standard for dose measurement.

Our analysis included three critical dose measurements in the FLASH regime: dose per pulse, average dose rate, and instantaneous dose rate. When conducting linear fitting of these measurements against RA signals, we observed a high level of linearity (with an  $R^2$  value exceeding 0.99), and no saturation was detected for doses per pulse up to 4.95 Gy. Figures 2(a)-(c) illustrate this linearity, showing single pulse RA signals and the relationship between RA signal amplitude and both the dose per pulse and the instantaneous dose rate. Further, our findings indicated no overlap in RA signals at different repetition frequencies, even up to 250 Hz, confirming time-of-flight predictions. This is crucial for understanding RA signal behavior in high repetition rate FLASH RT settings.

#### 3.2. Volumetric dose map for FLASH RT

Using a 256-element matrix array in water, we demonstrated the capability of RAI for 3D dose mapping in FLASH-RT. The array was placed in water facing upwards, parallel to the beam edges as shown in figure 1. A rectangular 3 cm × 4 cm collimator was utilized to shape the beam. As seen in figure 3, the 3D RAI image reconstructions and the maximum intensity projections in different planes give a visual representation of the beam deposition in water. Reconstructions were found to have a resolution of 2.5 mm via Full-Width Half-Maximum calculations utilizing a Gaussian-fit of the edge spread function in the *Z*-axis (Zhang *et al* 2023). Figure 4 displays the *XY*-plane, where the dose deposition from the electron beam appears as a shallow penetrating Gaussian beam, typical for a 5.4 MeV electron beam. We have conducted a Monte Carlo simulation using TOPAS planning software (Prusator *et al* 2017) to predict this dose deposition, and the results closely matched the observed data, as evidenced in figure 3. However, in the *XZ*-plane, the collimated beam profile shows some distortion, a consequence of the limited angle reconstruction challenge inherent in using a matrix array geometry.

One challenge for the translation of FLASH into the clinic is dose conformity of individual pulses, ensuring that the correct dose output is delivered to the correct region. When examining the individual pulses from the same location, fired in succession at FLASH dose rates, variation between pulse output can be shown. Consecutive individual pulses were reconstructed into volumetric dose deposition maps. Figure 4 and supplementary figure (video) depict the variability between pulses (2.2% in water), as captured by the RAI system. This variability in water can be accounted for by variations in beam output, usually found to be  $\pm 2\%$  in the Mobetron electron machine (Beddar 2005), thus demonstrating the real time 3D (4D) capabilities as well as capturing the small differences between individual pulses.

#### 3.3. Radiation induced acoustic imaging on animal tissue

To assess the clinical applicability of our Radiation-Induced Acoustic (RAI) system, the same matrix array previously used for RAI was employed on a rabbit cadaver. Ultrasound gel facilitated the transmission of RA waves from the animal's body to the transducer. Figure 5 shows volumetric reconstructions from an

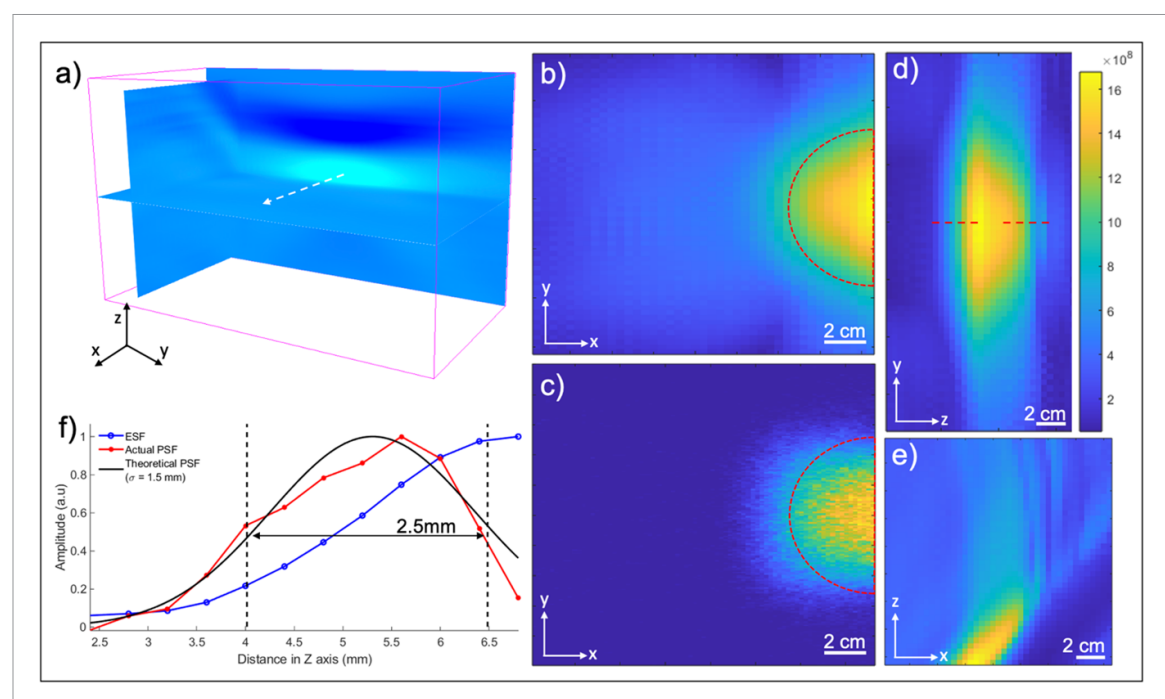


**Figure 3.** 3D volumetric dose mapping of FLASH electron beam in water. (a) displays a 3D reconstruction of the dose deposited by a 1.8  $\mu$ s pulse width beam, depicted by the white arrow, at a source-to-surface distance (SSD) of 450 mm within a water tank. The distribution of the dose across three dimensions is illustrated in the (b) X-Y plane, (d) Y-Z plane, and (e) X-Z plane. Panel (c) compares the dose deposition with a TOPAS simulation, demonstrating a strong correlation with the RAI-generated image in the X-Y plane. Graph (f) demonstrates the edge spread function or the reconstructed profile of the beam deposition taken at the red line in the Y-Z plane in (d). It further describes the finite-difference based derivative of the profile and its congruity with a Gaussian fitting, demonstrating the resolution to be 2.5 mm.

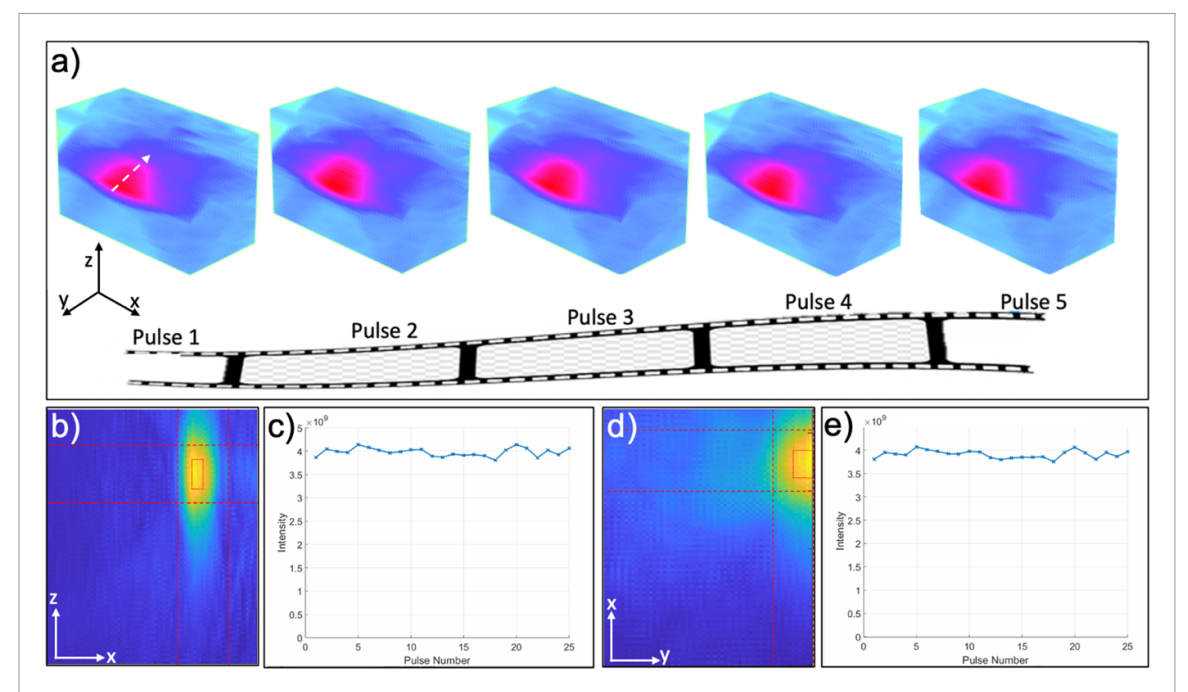


**Figure 4.** Real-time monitoring of dose variation in FLASH electron beam within water. (a) displays frames 1–5 capturing the electron beam's variations with each pulse, with an interval of 0.1 seconds between frames. Showcases the intensity fluctuation across pulses. The quantification of these changes is presented in (c) for the X–Z plane in (b) and in (e) for the X–Y plane, as seen in (d). A 2.2% variation between pulses was observed in the ROI. For a dynamic visualization, refer to the video in supplementary movie S1.

individual pulse. The initial beam deposition in the rabbit cadaver presented a low penetrating Gaussian shape in the *XY* plane, with noticeable hot spots due to tissue inhomogeneity. Consecutive RA signals generated from the rabbit chest were reconstructed, revealing variations in the volumetric dose distribution at the same distances for each individual pulse, as depicted in figure 6. The observed variability between

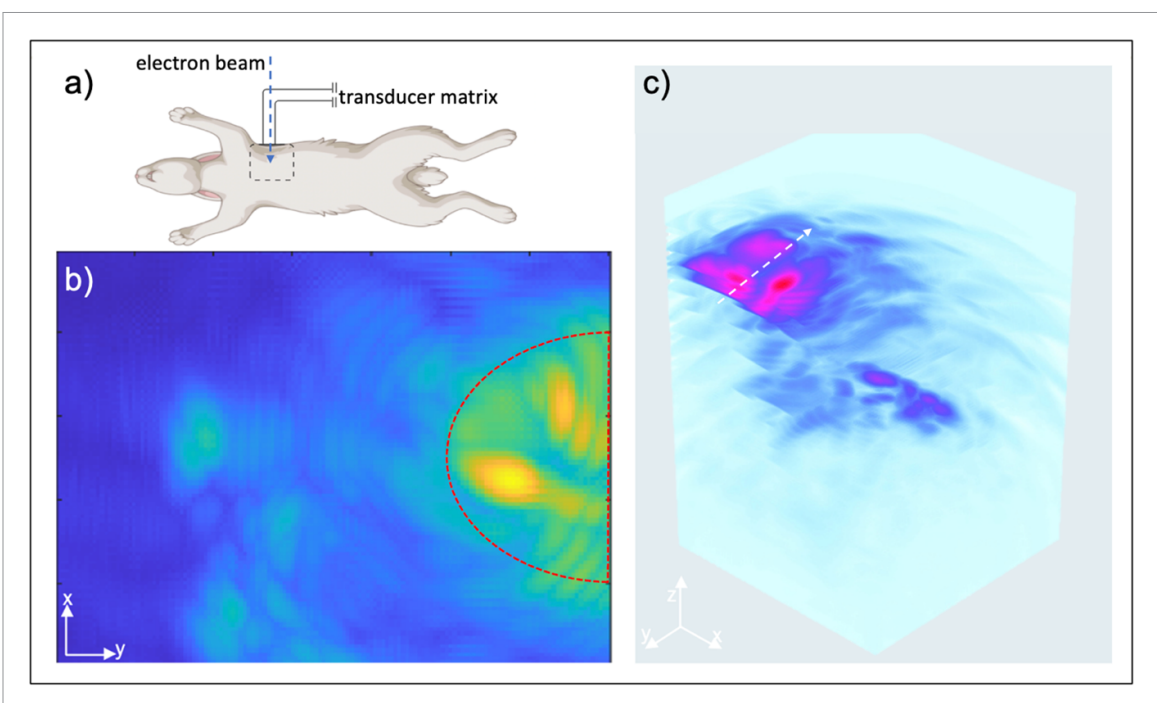


**Figure 5.** RAI imaging on rabbit model. (a) illustrates the positioning of the transducer underneath the chest with dotted lines. The beam irradiates the rabbit chest parallel to the transducer surface. (c) shows a 3D reconstruction of the dose delivered by a 1.8  $\mu$ s pulse width beam at a source-to-surface distance (SSD) of 450 mm into the rabbit chest. The maximum intensity projection in the *XY* plane (b) reveals beam penetration into rabbit tissue comparable to water, yet with notable hot spots arising from tissue heterogeneity.

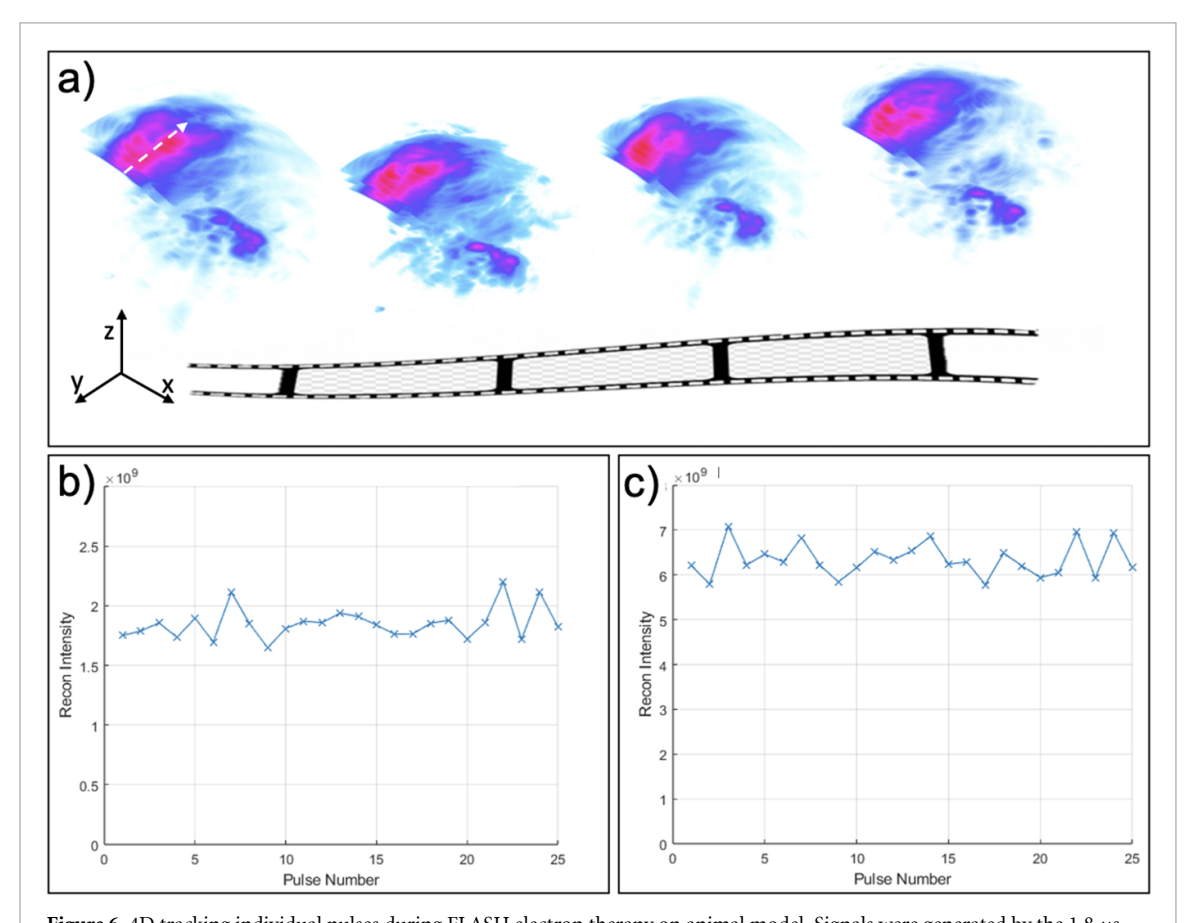


**Figure 6.** 4D tracking individual pulses during FLASH electron therapy on animal model. Signals were generated by the 1.8  $\mu$ s pulse width beam, depicted by the white arrow, depositing in the rabbit chest at a SSD of 450 mm. (a) shows 3D reconstruction of signals from individual consecutive pulses, demonstrating the feasibility of *in vivo* real-time monitoring and the ability to see variation in dose deposition from pulse to pulse. (b) utilizing a constrained ROI, variation between pulses was quantified in the X-Z plane (c) and the X-Y plane.

pulses was even more pronounced in tissue (5.88%) than in water due to tissue inhomogeneity. This not only underscores the importance of real-time volumetric monitoring in radiotherapy but also demonstrates the capability of RAI to provide effective 4D monitoring of radiotherapy treatments.

#### 4. Discussions

While RAI has been predominantly validated in conventional radiotherapy (Xiang et al 2012, Sampaio et al 2015, Kim et al 2017, Lei et al 2018, Samant et al 2020, Zheng et al 2020, Sun et al 2023, Zhang et al 2023), confirming its linearity in the FLASH regime is crucial. For the first time, we have extended RAI imaging to FLASH-RT, testing doses up to 5 Gy per pulse, which is 5000 times stronger than the doses typically used in conventional radiotherapy. Our results demonstrate that RAI maintains its linearity in this high-dose context, with an  $R^2$  value exceeding 0.99. Additionally, the RAI system's adjustable gain, ranging from 0 to 90 dB, allows for a broad coverage, accommodating both conventional radiotherapy doses (around 1 mGy per pulse) and the significantly higher doses used in FLASH-RT (up to 5 Gy per pulse). This versatility underscores the system's potential for diverse applications across different radiotherapy regimes.

We have successfully achieved 3D volumetric imaging for mapping radiation doses during FLASH-RT. Despite the encouraging outcomes of the RAI volumetric imaging system, there are areas that require further development. First, the system's spatial resolution requires improvement. Our results show a lateral resolution of 3 mm, limited by transducer size, and an axial resolution of about 2.5 mm, determined by the transducer's frequency bandwidth and electron pulse duration (Xiang *et al* 2016). This resolution is notably finer than previously reported (Zhang *et al* 2023), given our use of a 1 MHz frequency array and shorter radiation pulses (1.8  $\mu$ s). Lastly, the current UBP-based image reconstruction algorithm has limitations, especially evident in the distortion of beam edges in the *XZ* plane. We plan to develop deep learning algorithms to overcome these challenges (Jiang *et al* 2022, 2023, Lang *et al* 2023).

In vivo dose monitoring in heterogeneous tissues is vital for the clinical application of RAI in FLASH-RT. Figures 5 and 6 illustrate the system's capability for real-time, 3D monitoring of individual pulse dose deposition. In figure 5, a rabbit chest was irradiated, with the transducer coupled in the XY plane. The resulting maximum intensity projection reveals shallow dose deposition with variations due to tissue inhomogeneity. To further enhance our understanding of tissue variations, we intend to combine the RAI with ultrasound imaging in a dual-modal system (Patch *et al* 2016, Zhang *et al* 2020). Prior CT imaging will also be employed to refine reconstruction accuracy, a process readily applicable in clinical settings where CT scans are a standard part of treatment planning.

### 5. Conclusions

In conclusion, we have developed a RAI system that has successfully showcased the 4D imaging capabilities for dose mapping during FLASH-RT. It is capable of detecting doses as high as 5 Gy in a single pulse. Although there is room for improvement in both image reconstruction and quantitative dosimetry, the current system has enabled vital proof-of-concept experiments in both phantoms and animal tissue. These experiments demonstrate the potential of RAI in advancing the clinical application of FLASH-RT by accurately mapping dose deposition for individual pulses.

#### Data availability statement

The data cannot be made publicly available upon publication because they are not available in a format that is sufficiently accessible or reusable by other researchers. The data that support the findings of this study are available upon reasonable request from the authors.

#### Acknowledgments

The authors would like to acknowledge Ryan Johnson. Figure 5(a) was created with Biorender.com. This work was supported by the National Institute of Health (R37CA240806). The authors would also like to acknowledge the support from UCI Chao Family Comprehensive Cancer Center (P30CA062203). This work was supported by the Swiss National Science Foundation Grant (MAGIC—FNS CRS II5\_186369 to M-C V and supporting V G and R P and Spirit Grant IZSTZ0\_198747/1 to M-C V and P B-Z), Conacyt (P B-Z), NCI Grants P01CA244091 (M-C V and C L L).

#### Conflict of interest

The authors have no relevant conflict of interest to disclose.

#### **ORCID** iDs

Kristina Bjegovic https://orcid.org/0000-0002-9728-9124 Prabodh Pandey https://orcid.org/0000-0002-8962-2580

#### References

Ahmad M, Xiang L, Yousefi S and Xing L 2015 Theoretical detection threshold of the proton-acoustic range verification technique *Med. Phys.* 42 5735–44

Ashraf M R, Rahman M, Zhang R, Williams B B, Gladstone D J, Pogue B W and Bruza P 2020 Dosimetry for FLASH radiotherapy: a review of tools and the role of radioluminescence and Cherenkov emission *Front. Phys.* 8 328

Ba Sunbul N H et al 2021 A simulation study of ionizing radiation acoustic imaging (iRAI) as a real-time dosimetric technique for ultra-high dose rate radiotherapy (UHDR-RT) Med. Phys. 48 6137–51

Beddar A S 2005 Stability of a mobile electron linear accelerator system for intraoperative radiation therapy *Med. Phys.* **32** 3128–31 Bourhis J *et al* 2019 Treatment of a first patient with FLASH-radiotherapy *Radiother. Oncol. J. Eur. Soc. Ther. Radiol. Oncol.* **139** 18–22

Caron J, Gonzalez G, Pandey P K, Wang S, Prather K, Ahmad S, Xiang L and Chen Y 2023 Single pulse protoacoustic range verification using a clinical synchrocyclotron *Phys. Med. Biol.* **68** 045011

El Naqa I, Pogue B W, Zhang R, Oraiqat I and Parodi K 2022 Image guidance for FLASH radiotherapy Med. Phys. 49 4109–22

Glaser A K, Voigt W H A, Davis S C, Zhang R, Gladstone D J and Pogue B W 2013 Three-dimensional Čerenkov tomography of energy deposition from ionizing radiation beams *Opt. Lett.* **38** 634–6

Glaser A K, Zhang R, Gladstone D J and Pogue B W 2014 Optical dosimetry of radiotherapy beams using Cherenkov radiation: the relationship between light emission and dose *Phys. Med. Biol.* 59 3789–811

Gonzalez G, Prather K, Pandey P, Sun L, Caron J, Wang S, Ahmad S, Xiang L and Chen Y 2023 Single-pulse x-ray acoustic computed tomography image guided precision radiation therapy *Adv. Radiat. Oncol.* 8 101239

Hickling S, Hobson M and El Naqa I 2018a Characterization of x-ray acoustic computed tomography for applications in radiotherapy dosimetry IEEE Trans. Radiat. Plasma Med. Sci. 2 337–44

Hickling S, Xiang L, Jones K C, Parodi K, Assmann W, Avery S, Hobson M and El Naqa I 2018b Ionizing radiation-induced acoustics for radiotherapy and diagnostic radiology applications *Med. Phys.* 45 e707–21

Hu Y, Chen Z, Xiang L and Xing D 2019 Extended depth-of-field all-optical photoacoustic microscopy with a dual non-diffracting Bessel beam *Opt. Lett.* 44 1634

Jaccard M, Durán M T, Petersson K, Germond J-F, Liger P, Vozenin M-C, Bourhis J, Bochud F and Bailat C 2018 High dose-per-pulse electron beam dosimetry: commissioning of the Oriatron eRT6 prototype linear accelerator for preclinical use *Med. Phys.* 45 863–74

Jarvis L A, Zhang R, Gladstone D J, Jiang S, Hitchcock W, Friedman O D, Glaser A K, Jermyn M and Pogue B W 2014 Cherenkov video imaging allows for the first visualization of radiation therapy in real time *Int. J. Radiat. Oncol. Biol. Phys.* 89 615–22

Jiang Z, Sun L, Yao W, Wu Q J, Xiang L and Ren L 2022 3D *in vivo* dose verification in prostate proton therapy with deep learning-based proton-acoustic imaging *Phys. Med. Biol.* 67 215012

Jiang Z, Wang S, Xu Y, Sun L, Gonzalez G, Chen Y, Wu Q J, Xiang L and Ren L 2023 Radiation-induced acoustic signal denoising using a supervised deep learning framework for imaging and therapy monitoring *Phys. Med. Biol.* 68 235010

Kim J, Park E Y, Jung Y, Kim B C, Kim J H, Yi C-Y, Kim I J and Kim C 2017 X-ray acoustic-based dosimetry using a focused ultrasound transducer and a medical linear accelerator *IEEE Trans. Radiat. Plasma Med. Sci.* 1 534–40

Kim K, Pandey P K, Gonzalez G, Chen Y and Xiang L 2023 Simulation study of protoacoustics as a real-time in-line dosimetry tool for FLASH proton therapy *Med. Phys.* (https://doi.org/10.1002/mp.16894)

Lang Y, Jiang Z, Sun L, Xiang L and Ren L 2024 Hybrid-supervised deep learning for domain transfer 3D protoacoustic image reconstruction (arXiv:2308.06194)

Lao Y, Xing D, Yang S and Xiang L 2008 Noninvasive photoacoustic imaging of the developing vasculature during early tumor growth *Phys. Med. Biol.* 53 4203–12

Lei H, Zhang W, Oraiqat I, Liu Z, Ni J, Wang X and El Naqa I 2018 Toward *in vivo* dosimetry in external beam radiotherapy using x-ray acoustic computed tomography: a soft-tissue phantom study validation *Med. Phys.* 45 4191–200

Levy K et al 2020 Abdominal FLASH irradiation reduces radiation-induced gastrointestinal toxicity for the treatment of ovarian cancer in mice Sci. Rep. 10 21600

Mijnheer B, Beddar S, Izewska J and Reft C 2013 In vivo dosimetry in external beam radiotherapy Med. Phys. 40 070903

Montay-Gruel P et al 2021 Hypofractionated FLASH-RT as an effective treatment against glioblastoma that reduces neurocognitive side effects in mice Clin. Cancer Res. 27 775–84

Olaciregui-Ruiz I, Beddar S, Greer P, Jornet N, McCurdy B, Paiva-Fonseca G, Mijnheer B and Verhaegen F 2020 *In vivo* dosimetry in external beam photon radiotherapy: requirements and future directions for research, development, and clinical practice *Phys. Imaging Radiat. Oncol.* 15 108–16

Oraiqat I, Zhang W, Litzenberg D, Lam K, Ba Sunbul N, Moran J, Cuneo K, Carson P, Wang X and El Naqa I 2020 An ionizing radiation acoustic imaging (iRAI) technique for real-time dosimetric measurements for FLASH radiotherapy *Med. Phys.* 47 5090–101

Patch S K *et al* 2016 Thermoacoustic range verification using a clinical ultrasound array provides perfectly co-registered overlay of the Bragg peak onto an ultrasound image *Phys. Med. Biol.* **61** 5621–38

Prusator M, Ahmad S and Chen Y 2017 TOPAS Simulation of the Mevion S250 compact proton therapy unit J. Appl. Clin. Med. Phys. 18 88–95

Samant P, Trevisi L, Ji X and Xiang L 2020 X-ray induced acoustic computed tomography Photoacoustics 19 100177

Sampaio D R T, Uliana J H, Carneiro A A O, Pavoni J F, Pavan T Z and Borges L F 2015 X-ray acoustic imaging for external beam radiation therapy dosimetry using a commercial ultrasound scanner 2015 IEEE Int. Ultrasonics Symp. (IUS) (IEEE) pp 1–4

Simmons D A et al 2019 Reduced cognitive deficits after FLASH irradiation of whole mouse brain are associated with less hippocampal dendritic spine loss and neuroinflammation Radiother. Oncol. J. Eur. Soc. Ther. Radiol. Oncol. 139 4–10

Soto L A *et al* 2020 FLASH irradiation results in reduced severe skin toxicity compared to conventional-dose-rate irradiation *Radiat. Res.* 194 618–24

Sun L, Gonzalez G, Pandey P K, Wang S, Kim K, Limoli C, Chen Y and Xiang L 2023 Towards quantitative in vivo dosimetry using x-ray acoustic computed tomography Med. Phys. 50 16476

Vozenin M C et al 2019 The advantage of FLASH radiotherapy confirmed in mini-pig and cat-cancer patients Clin. Cancer Res. Off. J. Am. Assoc. Cancer Res. 25 35–42

Wang B, Xiang L, Jiang M S, Yang J, Zhang Q, Carney P R and Jiang H 2012 Photoacoustic tomography system for noninvasive real-time three-dimensional imaging of epilepsy *Biomed. Opt. Express* 3 1427

Wang LV and HuS 2012 Photoacoustic tomography: in vivo imaging from organelles to organs Science 335 1458-62

Wang M, Samant P, Wang S, Merill J, Chen Y, Ahmad S, Li D and Xiang L 2020 Towards *in vivo* dosimetry for prostate radiotherapy with a transperineal ultrasound array: a simulation study *IEEE Trans. Radiat. Plasma Med. Sci.* 5 373–82

Xiang L, Han B, Carpenter C, Pratx G, Kuang Y and Xing L 2012 X-ray acoustic computed tomography with pulsed x-ray beam from a medical linear accelerator Med. Phys. 40 010701

Xiang L, Tang S, Ahmad M and Xing L 2016 High resolution x-ray-induced acoustic tomography Sci. Rep. 6 26118

Xiang L, Wang B, Ji L and Jiang H 2013 4-D photoacoustic tomography Sci. Rep. 3 1113

Xiang L, Yuan Y, Xing D, Ou Z, Yang S and Zhou F 2009 Photoacoustic molecular imaging with antibody-functionalized single-walled carbon nanotubes for early diagnosis of tumor *J. Biomed. Opt.* 14 021008

Xu M and Wang L V 2005 Universal back-projection algorithm for photoacoustic computed tomography *Phys. Rev.* E 71 016706
Yan Y and Xiang S L 2024 X-ray-induced acoustic computed tomography and its applications in biomedicine *J. Biomed. Opt.* 29 S11510

Yang D W, Xing D, Yang S H and Xiang L Z 2007a Fast full-view photoacoustic imaging by combined scanning with a linear transducer array Opt. Express 15 15566

Yang S, Xing D, Zhou Q, Xiang L and Lao Y 2007b Functional imaging of cerebrovascular activities in small animals using high-resolution photoacoustic tomography: photoacoustic imaging of cerebrovascular activities *Med. Phys.* 34 3294–301

Zeng L, Xing D, Gu H, Yang D, Yang S and Xiang L 2007 High antinoise photoacoustic tomography based on a modified filtered backprojection algorithm with combination wavelet *Med. Phys.* 34 556–63

Zhang W et al 2023 Real-time, volumetric imaging of radiation dose delivery deep into the liver during cancer treatment Nat. Biotechnol. 41 1160–7

Zhang W, Oraiqat I, Lei H, Carson P L, Ei Naqa I and Wang X 2020 Dual-modality x-ray-induced radiation acoustic and ultrasound imaging for real-time monitoring of radiotherapy *BME Front.* 2020 9853609

Zheng Y, Samant P, Merill J, Chen Y, Ahmad S, Li D and Xiang L 2020 X-ray-induced acoustic computed tomography for guiding prone stereotactic partial breast irradiation: a simulation study *Med. Phys.* 47 4386–95